

RED STAR FORMING GALAXIES AND THEIR ENVIRONMENT AT $Z = 0.4$ REVEALED BY PANORAMIC H α IMAGING

YUSEI KOYAMA¹, TADAYUKI KODAMA^{2,3}, FUMIAKI NAKATA^{2,3}, KAZUHIRO SHIMASAKU^{1,4} AND SADANORI OKAMURA^{1,4}

¹Department of Astronomy, School of Science, The University of Tokyo, Tokyo 113-0033, Japan

²National Astronomical Observatory of Japan, Mitaka, Tokyo 181-8588, Japan

³Subaru Telescope, National Astronomical Observatory of Japan, 650 North A'ohoku Place, Hilo, HI 96720, USA and

⁴Research Center for the Early Universe, School of Science, The University of Tokyo, Tokyo 113-0033, Japan

Accepted for publication in ApJ

ABSTRACT

We present a wide-field H α imaging survey of the rich cluster CL0939+4713 (Abell 851) at $z = 0.41$ with Suprime-Cam on the Subaru Telescope, using the narrow-band filter NB921. The survey is sensitive to active galaxies with star formation rates down to $\sim 0.3M_{\odot}/\text{yr}$ throughout the $27' \times 27'$ field, and we identified 445 H α emitters along the large-scale structures around the cluster. Using this sample, we find that (1) the fraction of H α emitters is a strong function of environment and shows a clear decline toward the cluster central region. We also find that (2) the color of H α emitters is clearly dependent on environment. The majority of the H α emitters have blue colors with $B - I < 2$, but we find H α emitters with red colors as well. Such red emitters are very rare in the cluster center or its immediate surrounding regions, while they are most frequently found in groups located far away from the cluster center. These groups coincide with the environment where a sharp transition in galaxy color distribution is seen. This may suggest that dusty star formation activity tends to be involved in galaxy truncation processes that are effective in groups, and it is probably related to the “pre-processing” that generates present-day cluster S0 galaxies. Finally, we confirm that (3) the mass-normalized integrated star formation rate in clusters (i.e. the total star formation rate within $0.5 \times R_{200}$ from the cluster center divided by the cluster dynamical mass) rapidly increases with look-back time following approximately $\propto (1+z)^6$, and it is also correlated with the cluster mass.

Subject headings: galaxies: evolution, galaxies: active, galaxies: clusters: individual (Abell 851)

1. INTRODUCTION

It has long been known that properties of galaxies are strongly correlated with environment where galaxies reside. Clusters of galaxies are dominated by red early-type galaxies with little star forming activity, while the dominant population in the low-density field are blue late-type galaxies with significant star formation (e.g. Dressler 1980; Lewis et al. 2002; Gómez et al. 2003). It is suspected that the growth of large-scale structures comes into play and alters galaxy properties during the course of hierarchical assembly. However, it is not yet clear what physical process(es) is (are) actually responsible for shaping galaxy properties depending on the environment. Distant clusters of galaxies, which tend to be in an active phase of mass assembly, are ideal sites for studying “directly” what is really happening along with the cluster growth.

Cosmological simulations predict that galaxies and groups are assembled onto massive clusters moving along filamentary structures (e.g. Millennium Simulation; Springel et al. 2005), and in fact, wide-field observations of distant clusters of galaxies have revealed such filamentary large-scale structures around rich clusters up to $z \sim 1.3$ (e.g. Kodama et al. 2005; Tanaka et al. 2007). Those cluster surrounding regions including infalling groups and/or filamentary structures are likely to be playing critical roles in the evolution of cluster galaxies. It is reported that the rest-frame ultra-violet(UV)–optical colors change sharply from blue to red in such

medium density environments (e.g. Kodama et al. 2001; Tanaka et al. 2005; Koyama et al. 2008), suggesting that at least a part of the star forming activities of cluster red galaxies are quenched through some environmental effects *before* entering the cluster core region. However, optical colors do not necessarily provide us with the full picture of star forming activities of galaxies. In fact, some “red” galaxies involve, despite of their red colors, a significant amount of dust-obscured star-formation activity (e.g. Wolf et al. 2005; 2009; Davoodi et al. 2006; Koyama et al. 2008; 2010; Haines et al. 2008; Verdugo et al. 2008; Gallazzi et al. 2009; Mahajan & Raychaudhury 2009; Brand et al. 2009). Such galaxies might be the key population in the “transition phase” from blue active galaxies to red quiescent ones. Therefore, it is crucial to quantify star formation activity more robustly using not only colors but also other independent indicators of star formation.

For this purpose, H α emission line ($\lambda_{\text{rest}} = 6563\text{\AA}$) is of great use as it is one of the best indicators of star formation which directly reflects the UV radiation from O- and B-type stars in the HII regions and is very well calibrated with local galaxies (Kennicutt 1998). Also, the H α line is much less affected by dust extinction or metallicity effect compared to [OII] lines at a shorter wavelength ($\lambda_{\text{rest}} = 3727\text{\AA}$) or UV–optical colors, which are more commonly used in the studies of galaxies in the distant Universe.

Taking the great advantage of the wide field of view of Suprime-Cam (Miyazaki et al. 2002) on Subaru Telescope (Iye et al. 2004), panoramic narrow-band imag-

ing of $H\alpha$ emitters in the distant cluster environment was first conducted by Kodama et al. (2004), who targeted the CL0024+16 cluster at $z = 0.39$ over a $\sim 27' \times 27'$ area centered on the cluster. Following this study, Koyama et al. (2010) conducted wide-field narrow-band imaging of $H\alpha$ emitters in and around the RXJ1716+6708 cluster at $z = 0.81$. They used the wide-field near-infrared camera, MOIRCS (Ichikawa et al. 2006; Suzuki et al. 2008), on the Subaru Telescope, and spent 8 pointings to neatly cover the known filamentary structures found by Koyama et al. (2007). Finn et al. (2004) and Finn et al. (2005) also performed $H\alpha$ emitter surveys in the central regions of several EDisCS clusters at $z \sim 0.6$ – 0.8 (EDisCS: White et al. 2005). More recently, Sobral et al. (2011) studied environmental dependence of star forming activity at $z \sim 0.8$ based on their $H\alpha$ emitters sample from HiZELS (which includes several clusters in the COSMOS and the UKIDSS UDS fields). In spite of the great importance of $H\alpha$ surveys of clusters and their surrounding regions to investigate the environmental effects, the number of $H\alpha$ surveys of clusters has still been very limited. Since clusters of galaxies are statistical objects by nature, we desperately need more $H\alpha$ -based studies of distant clusters that cover a wide area and a long time baseline in order to discuss the environmental variation of star forming galaxies and its evolution.

In this paper, we present a $H\alpha$ emitter survey for another cluster at $z \sim 0.4$, CL0939+4713 (Abell 851). This is a very rich cluster and is one of the most famous intermediate redshift clusters. Intensive imaging/spectroscopic surveys of this cluster including the *MORPHS* survey (Smail et al. 1997) have been made by many authors, which include ground-based broad-band imaging (e.g. Dressler & Gunn 1992; Stanford et al. 1995; Iye et al. 2000; Kodama et al. 2001), narrow-band imaging (Belloni et al. 1995; Martin et al. 2000), optical spectroscopy (e.g. Dressler et al. 1999; Sato & Martin 2006ab; Oemler et al. 2009; Nakata et al. 2011), Hubble Space Telescope imaging including UV observation (e.g. Dressler et al. 1994ab; Smail et al. 1999; Buson et al. 2000), Spitzer mid-infrared imaging (Dressler et al. 2009), sub-millimeter $850\mu\text{m}$ observation (Cowie et al. 2002) and VLA radio observation (Smail et al. 1999). This cluster has also been targeted by X-ray observations several times (Schindler & Wambsganss 1996; Schindler et al. 1998; De Filippis et al. 2003). The X-ray image of this cluster shows two prominent peaks in X-ray emission, which suggests that the Abell 851 cluster is a dynamically young system.

The structure of this paper is as follows. In Section 2, we summarize our project and the concept of this paper. In Section 3, we show the selection technique of $H\alpha$ emitters at $z = 0.4$ and the derivation of $H\alpha$ -derived star-formation rates for the selected $H\alpha$ emitters. Our main results and discussions are described in Sections 4–6, and we summarize our results in Section 7. Throughout this paper, we assume $\Omega_M = 0.3$, $\Omega_\Lambda = 0.7$, and $H_0 = 70 \text{ km s}^{-1} \text{ Mpc}^{-1}$, which gives a $1''$ scale of 5.41 kpc at the most up-to-date redshift of the Abell 851 cluster ($z = 0.405$; Oemler et al. 2009). Magnitudes are all given in the AB system.

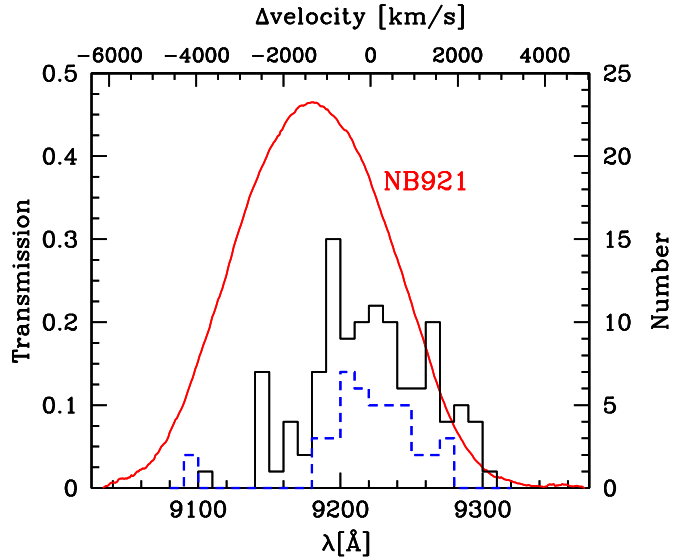


FIG. 1.— The transmission curve of the NB921 filter, including the response of the CCD. The histograms show the distribution of the line-of-sight velocity relative to the velocity center and the corresponding observed wavelength of $H\alpha$ lines for spectroscopically confirmed cluster member galaxies. The solid-line histogram is for galaxies near the cluster center and the dashed-line histogram is for galaxies far away from the cluster, taken from Oemler et al. (2009) and Nakata et al. (2011), respectively.

2. DATA

2.1. PISCES project

We have been conducting the Panoramic Imaging and Spectroscopy of Cluster Evolution with Subaru project (PISCES: Kodama et al. 2005). We widely observed X-ray detected rich clusters at $0.4 \lesssim z \lesssim 1.4$ mainly using Suprime-Cam on the Subaru Telescope, and discovered prominent large-scale structures around each cluster (Kodama et al. 2001; Tanaka et al. 2005; 2006; 2007ab; 2008; 2009ab; Nakata et al. 2005; Koyama et al. 2007; 2008). We also conducted wide-field mapping of star formation around several clusters by $H\alpha$ or $[\text{OII}]$ line using available narrow-band filters installed on the Suprime-Cam or MOIRCS (Kodama et al. 2004; Koyama et al. 2010; Hayashi et al. 2010; 2011). The narrow-band imaging survey is powerful in the sense that it enables us to conduct a very complete survey of star forming activity in and around clusters. We can detect emission lines by imaging observations and can measure the line flux throughout the field at the same time (see also Section 3.1).

2.2. This study

As a pioneering survey of our PISCES project, the Abell 851 cluster was studied by Kodama et al. (2001). They performed *BVRI* imaging of this cluster with Suprime-Cam covering $27' \times 27'$ field and found prominent large-scale structures using the photometric redshift technique. Nakata et al. (2011) performed a wide-field spectroscopic follow-up observation and confirmed that these huge structures are really at the same redshift as of the main cluster. Fortunately, the $H\alpha$ line from Abell 851 shifts to $\simeq 9220\text{\AA}$ which is between the night sky emission lines. We utilize a narrow-band filter NB921

($\lambda_c = 9180\text{\AA}$, $\Delta\lambda = 133\text{\AA}$) installed on the Suprime-Cam, and using this filter we conduct a wide-field H α emitter survey for this cluster. The transmission curve of the NB921 filter is shown in Fig. 1 with the velocity distribution of spectroscopically confirmed cluster member galaxies taken from Oemler et al. (2009) (solid-line histogram). We also show the velocity distribution of member galaxies in the filamentary structures located far away from the cluster center taken from Nakata et al. (2011) (dashed-line histogram). No significant difference can be seen between the two distributions, supporting that our narrow-band survey is uniformly sensitive throughout the field. We also note that the peak of the velocity distribution and that of the filter transmission are slightly different. We can still detect H α emission from cluster member galaxies with the line-of-sight velocities of $-3500\text{km/s} \lesssim \Delta v \lesssim +1000\text{km/s}$, although we need to be careful when deriving physical quantities such as star formation rates (SFRs). Nevertheless, this filter is sensitive to $\gtrsim 70\%$ of H α emission lines of member galaxies throughout the field, and this provides us with a great opportunity to conduct a wide-field H α emitter survey in and around the Abell 851 cluster.

On top of the Suprime-Cam *BVRI* imaging data and photometric redshifts (phot- z) of the Abell 851 cluster field taken from Kodama et al. (2001), we have also collected z' -band and NB921 data using Suprime-Cam covering the same area as the existing *BVRI* imaging data (i.e. $27' \times 27'$). The data are reduced in a standard manner using the Suprime-Cam data reduction pipeline (Yagi et al. 2002; Ouchi et al. 2004) in the same way as described in Kodama et al. (2001), and all the images are smoothed to $\simeq 1.1''$ seeing size, which is the worst seeing among our data (the *B*-band data). The exposure times are 30 min and 180 min for z' -band and NB921, respectively, and the 5σ limiting magnitudes are 24.0 mag and 24.4 mag, respectively (measured from the deviation of randomly distributed $3''$ apertures in each image). Photometry of sources is performed at the position of *I*-band detected objects with $I \leq 24.0\text{mag}$ ($= M_V^* + 4$) using SExtractor software (Bertin & Arnouts 1996), and we use $3''$ aperture photometry throughout the paper.

3. ANALYSIS

3.1. H α emitter selection

We first identify narrow-band excess galaxies using the z' -NB921 colors. We plot in Fig. 2 the z' -NB921 colors of all galaxies within the observed field against their NB921 magnitudes. The curves show $\pm 3\sigma$ color excesses. We define the NB921 emitters as those satisfying $z' - \text{NB921} > 0.2$ and $z' - \text{NB921} > 3\sigma$ (see the magenta crosses above the $z' - \text{NB921} = 0.2$ line and $z' - \text{NB921} = +3\sigma$ curve in Fig. 2). We detect 724 NB921 emitters in total, but a part of these emitters are not necessarily H α emitters at $z = 0.4$ since H β /[OIII] emitters at $z \sim 0.8$ and [OII] emitters at $z \sim 1.45$ can also be detected as NB921 emitters. However, these contaminations can be relatively easily eliminated based on their broad-band colors. In Fig. 3, we show the *B* - *R* v.s. *R* - z' color-color diagram. We here plot galaxies with $0.30 < z_{\text{phot}} < 0.45$ (gray dots) and all the NB921 emitters selected above (magenta crosses). We also show the model prediction of colors for galaxies at $z = 0.4, 0.8$ and

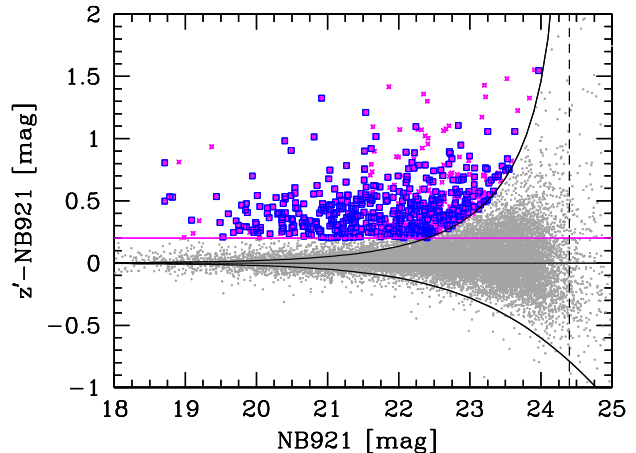


FIG. 2.— The plot showing our selection method of the NB921 emitters. The $z' - \text{NB921}$ colors are plotted against NB921 magnitudes. The vertical dashed line indicates the 5σ limiting magnitude for NB921, and the solid-line curves show the $\pm 3\sigma$ excesses in $z' - \text{NB921}$ colors. Galaxies with $z' - \text{NB921} > 0.2$ and $z' - \text{NB921} > 3\sigma$ are defined as NB921 emitters (magenta crosses). The blue squares indicate the H α emitters at $z \sim 0.4$ selected in Fig. 3 (i.e. NB921 emitters in the blue-line box in Fig. 3).

1.45 from Kodama et al. (1999). This color combination clearly separates the H α emitters at $z \sim 0.4$ from other major line emitters at other redshifts, and in fact, these colors are also used in Kodama et al. (2004) in order to identify H α emitters at a similar redshift ($z = 0.39$). We define the NB921 emitters distributed in the closed box in Fig. 3 as H α emitters at $z = 0.4$. We note that this boundary is set by eye, and we may miss a small fraction of real members near the boundary. However, a small change of this boundary does not change our results at all (see similar selection method in Kodama et al. 2004 and Koyama et al. 2010). Also, this color selection can be applied only for the galaxies that are detected in all *BRz'*-bands. Therefore, we do not include any H α emitter if it is not detected in any of these bands. However, the quantitative analyses presented in this paper are mainly based on bright galaxies with $z' < 23$ mag, and are not affected by the faint undetected objects. After application of all these color cuts, we are left with 445 H α emitters in total in and around the Abell 851 cluster throughout the observed field. This is one of the largest samples of H α emitters currently available for distant clusters.

3.2. Necessity of narrow-band imaging

We here briefly describe the powerfulness of the narrow-band survey. We show a plot showing z_{spec} v.s. z_{phot} in Fig. 4. The spectroscopic catalog of the Abell 851 field is taken from Oemler et al. (2009). The photometric redshifts are not always perfect, especially for blue star forming galaxies due to the lack of significant features such as 4000 \AA break in their spectral energy distribution (SED) (e.g. Kodama et al. 1999). In fact, as can be seen in Fig. 4, our photometric redshifts for blue member galaxies sometimes fail and return significantly lower redshifts (see the inset of Fig. 4). This color dependence of the phot- z accuracy makes it difficult to study star forming activity and/or its dependence on environment. In

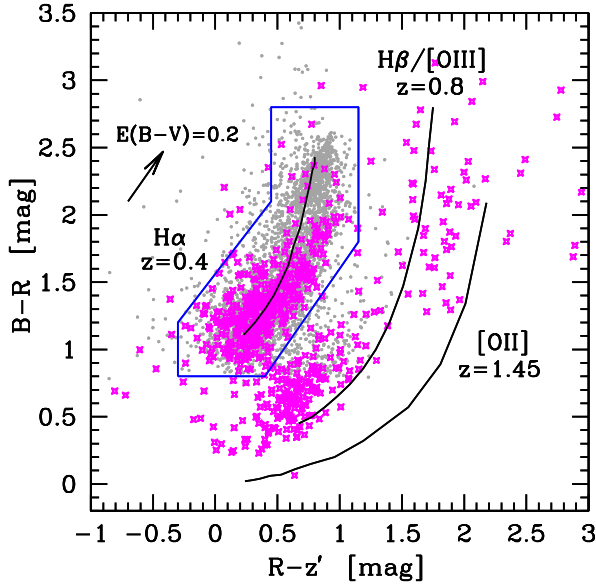


FIG. 3.— The color-color diagram to separate $H\alpha$ emitters at $z = 0.4$ from other major line contaminations at other redshifts ($H\beta/[OIII]$ emitters at $z \sim 0.8$ and $[OII]$ emitters at $z \sim 1.45$). Gray dots represent phot- z selected member galaxies and magenta crosses indicate all NB921 emitters selected in Fig. 2. Three solid-line curves indicate color tracks of galaxies at $z=0.4$, 0.8 and 1.45 , based on the model prediction of Kodama et al. (1999). Along each track, we change the fraction of bulge contribution to the total light from 0.0 to 1.0 (from blue side to red side). We define the NB921 emitters (i.e. magenta crosses) within the blue-line closed box as $H\alpha$ emitters at $z = 0.4$, while emitters outside the box as contaminant line emitters. We also show the reddening vector corresponding to $E(B-V) = 0.2$ for $z = 0.4$ galaxies, calculated from the extinction law of Calzetti et al. (2000).

contrast, narrow-band surveys detect emission lines as an excess of flux at a certain wavelength, and in fact, many of the real members missed in the phot- z selection can be *rescued* in our narrow-band survey (see the squares in the inset of Fig. 4). Thus, we again stress that a more complete sample of star-forming galaxies can be constructed regardless of their colors, through the narrow-band survey (see also the discussion in Kodama et al. 2004).

3.3. $H\alpha$ -derived star formation rate

Then, we estimate the star formation rates (SFR) for all the $H\alpha$ emitters selected above. At first, we calculate the $H\alpha + [NII]$ line flux ($F_{H\alpha+[NII]}$), continuum flux density (f_c) and rest-frame equivalent width (EW_R) in the following equations:

$$F_{H\alpha+[NII]} = \Delta_{NB} \frac{f_{NB} - f_{z'}}{1 - \Delta_{NB}/\Delta_{z'}} \quad (1)$$

$$f_c = \frac{f_{z'} - f_{NB}(\Delta_{NB}/\Delta_{z'})}{1 - \Delta_{NB}/\Delta_{z'}} \quad (2)$$

$$EW_R(H\alpha + [NII]) = (1+z)^{-1} \frac{F_{H\alpha+[NII]}}{f_c} \quad (3)$$

where $\Delta_{z'}$ ($= 955\text{\AA}$) and Δ_{NB} ($= 133\text{\AA}$) are the FWHMs of the z' and NB921 filters, $f_{z'}$ and f_{NB} are the flux densities at z' -band and at NB921, respectively. We then multiply $4\pi d_L^2$ by $F_{H\alpha+[NII]}$ to derive the luminosity $L(H\alpha +$

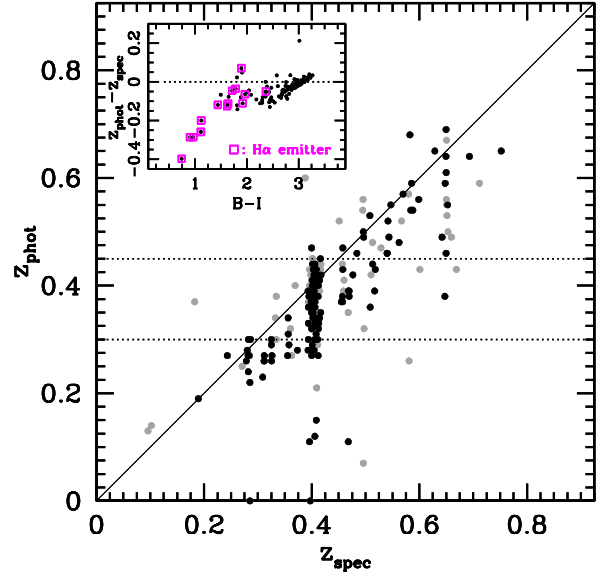


FIG. 4.— The z_{spec} v.s. z_{phot} plot for galaxies in the Abell 851 field. Spectroscopic data are taken from Table 1 of Oemler et al. (2009). Black and gray symbols indicate the galaxies with $Q=1,2$ and $Q=3,4$, respectively, where Q means the quality of the spectra (smaller Q means better quality; Oemler et al. 2009). The horizontal dotted lines show the phot- z member selection criteria used in this paper. In the inset, we show the accuracies of our photometric redshifts for spectroscopic members (i.e. $0.38 \leq z_{spec} \leq 0.42$) as a function of $B-I$ color. Open squares indicate $H\alpha$ emitters selected in Section 3.1. Photometric redshifts sometimes return lower values for blue galaxies, but it is evident that they are neatly recovered as the $H\alpha$ emitters.

$[NII]$), where d_L is the luminosity distance of 2204 Mpc at $z = 0.405$.

Finally, we compute the $H\alpha$ -based star formation rates, $SFR(H\alpha)$, using the Kennicutt (1998) relation for Salpeter (1955) IMF: $SFR(H\alpha)[M_\odot/\text{yr}] = 7.9 \times 10^{-42} L_{H\alpha}[\text{erg/s}]$. We correct for 30% $[NII]$ line contribution (e.g. Tresse et al. 1999) and consider 1 mag extinction in $H\alpha$ flux due to dust (e.g. Kennicutt & Kent 1983; Kennicutt 1992), following our previous studies (Kodama et al. 2004; Koyama et al. 2010). Our selection criteria of $H\alpha$ emitters shown in Section 3.1 correspond to $EW_R(H\alpha + [NII]) \gtrsim 20\text{\AA}$ and $SFR(H\alpha) \gtrsim 0.3 M_\odot/\text{yr}$, and the typical uncertainty in the $SFR(H\alpha)$ from photometric error is $\sim 0.1 M_\odot/\text{yr}$. We should note that the assumptions for $[NII]$ contamination and dust extinction adopted above are somewhat uncertain. It is reported that the contribution of $[NII]$ emission to the $H\alpha + [NII]$ line flux depends on $EW(H\alpha + [NII])$ (e.g. Villar et al. 2008) or B-band luminosity (Kennicutt et al. 2008). Also, the strength of dust extinction can vary a lot (e.g. depending on the morphological type of galaxies: Boselli et al. 2001), and in the extreme cases, it may become $A(H\alpha) \gtrsim 3\text{mag}$ (e.g. Poggianti & Wu 2000), although the assumption of ~ 1 mag extinction adopted here seems to be valid on average in the distant Universe as well and the level of dust extinction at a given SFR does not change strongly with redshift (e.g. Garn et al. 2010; Moore et al. 2010).

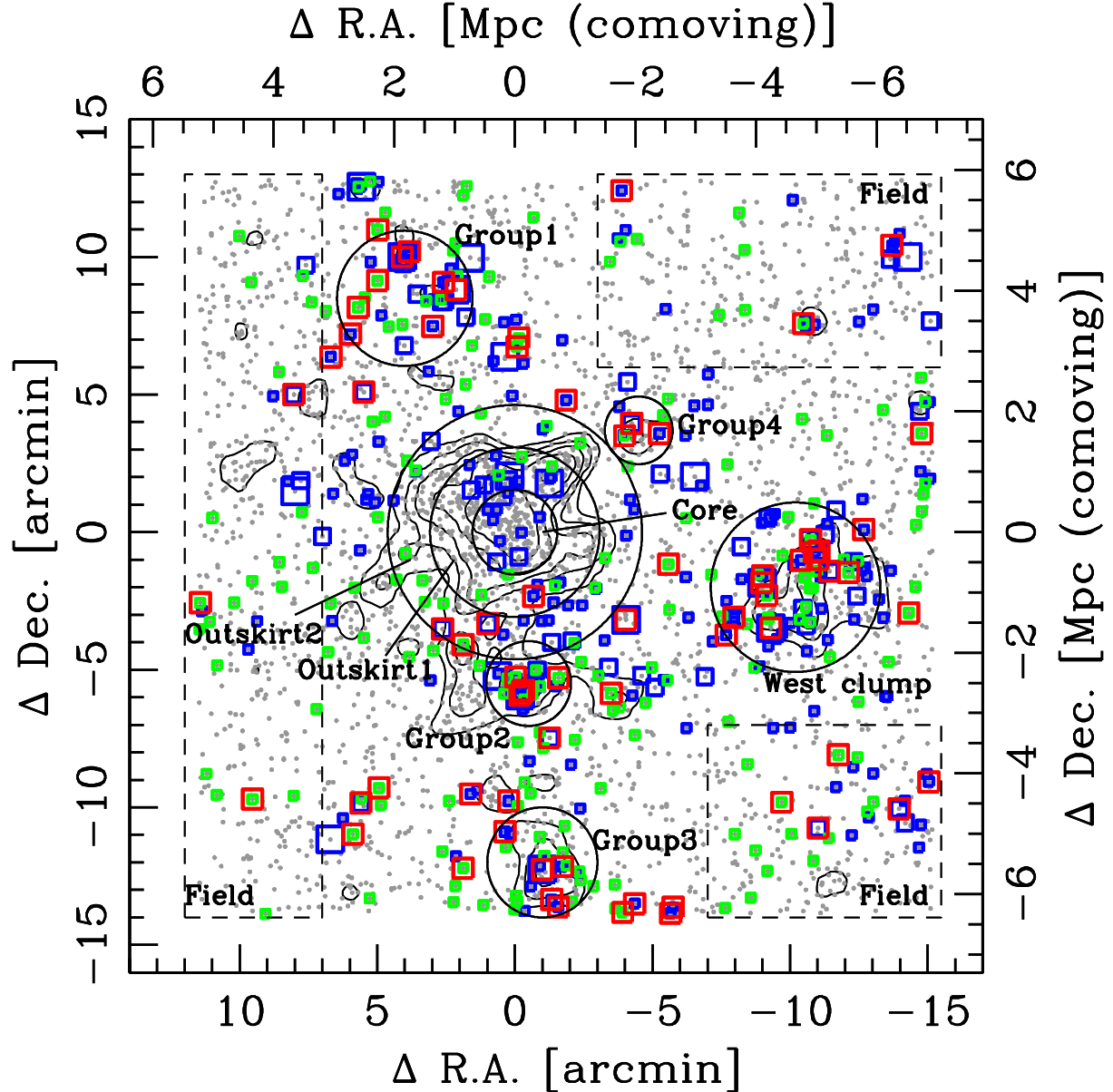


FIG. 5.— Spatial distribution of the phot- z members with $0.30 < z_{\text{phot}} < 0.45$ (gray dots) and $\text{H}\alpha$ emitters (open colored squares). Blue squares indicate $\text{H}\alpha$ emitters with $\text{SFR}_{\text{H}\alpha} > 0.75 \text{ M}_{\odot}/\text{yr}$ and larger symbols indicate galaxies with larger SFRs. Green squares show weak $\text{H}\alpha$ emitters with $\text{SFR}_{\text{H}\alpha} < 0.75 \text{ M}_{\odot}/\text{yr}$. Red squares represent the red $\text{H}\alpha$ emitters with $B - I > 2.0$. Contours show 3, 5, 7, 10, and 15σ significance of galaxy overdensity calculated using all the member galaxies (all the phot- z members and/or $\text{H}\alpha$ emitters). Solid-line circles and dashed-line rectangles show the areas where we define different environments to study environmental effects (see text and Table 1).

4. WIDE-FIELD MAPPING OF $\text{H}\alpha$ EMITTERS

4.1. Panoramic $\text{H}\alpha$ view of the Abell 851 cluster

We show in Fig. 5 the spatial distribution of the $\text{H}\alpha$ emitters selected in the previous section. The coordinates are shown with respect to the peak of the diffuse X-ray emission from the intra-cluster medium (R.A. = $09^{\text{h}}42^{\text{m}}58^{\text{s}}.0$ and Dec. = $+46^{\circ}59'01''$), which is the same definition as in Oemler et al. (2009). We plot all the cluster member candidates ($0.30 \leq z_{\text{phot}} \leq 0.45$; see the horizontal dotted-lines in Fig. 4) with gray dots. The $\text{H}\alpha$ emitters are shown by colored symbols in Fig. 5. Larger blue squares indicate larger star formation rates, and green squares indicate the galaxies with weak $\text{H}\alpha$

lines ($\text{SFR}_{\text{H}\alpha} < 0.75 \text{ M}_{\odot}/\text{yr}$). Also, we marked red squares for $\text{H}\alpha$ emitters with $B - I > 2.0$ (hereafter red $\text{H}\alpha$ emitters). Our survey revealed the entire distribution of star forming galaxies around the Abell 851 cluster across the $\sim 30'$ field for the first time. It is evident that the $\text{H}\alpha$ emitters are widely distributed throughout the field, which strongly supports the existence of real structures at $z = 0.41$ associated with the central cluster Abell 851. In fact, most of the structures have been spectroscopically confirmed to be physically associated to the cluster based on our intensive spectroscopic follow-up (Nakata et al. 2011).

We here define the galaxy environment used in this

TABLE 1
DEFINITION OF ENVIRONMENT AROUND ABELL 851.

Name	R.A. (J2000)	Dec. (J2000)	Δ R.A. (arcmin)	Δ Dec. (arcmin)	radius (Mpc)
Core.....	09 42 58.0	+46 59 01	0.0	0.0	0.5
Outskirt-1.....	09 42 58.0	+46 59 01	0.0	0.0	0.5–1.0
Outskirt-2.....	09 42 58.0	+46 59 01	0.0	0.0	1.0–1.5
West Clump.....	09 41 57.7	+46 56 56	−10.2	−2.0	1.0
Group-1.....	09 43 21.5	+47 07 37	4.0	8.5	0.8
Group-2.....	09 42 55.2	+46 53 28	−0.5	−5.5	0.5
Group-3.....	09 42 52.4	+46 46 54	−1.0	−12.0	0.65
Group-4.....	09 42 31.2	+47 02 44	−4.5	3.7	0.4

NOTE. — Δ R.A. and Δ Dec. are the central coordinates of each environment relative to the cluster center.

paper as shown in Fig. 5, and summarize them in Table 1. The cluster core and outskirts regions (1 and 2) correspond to $r_c < 0.5$ Mpc (which include the two X-ray emission peaks; see Oemler et al. 2009), $0.5 < r_c < 1.0$ Mpc and $1.0 < r_c < 1.5$ Mpc from the cluster center, respectively (all in the physical scale). We also define the West clump (the richest group in the observed field) and Group-1,2,3, and 4 to pick out galaxies concentrated in groups relatively far out from the cluster core. Note that the West clump, Group-2 and 3 are large clumps spectroscopically confirmed by Nakata et al. (2011), while the Group-1 region was not well covered by their spectroscopic observation. The Group-4 is also a spectroscopically confirmed in-falling group (which is identical to the NW group in Oemler et al. 2009). It is interesting to note that in addition to these known structures (West clump, Group-2,3,4) H α emitters are concentrated in the northern part (i.e. Group-1), where we did not identify a prominent overdensity of phot- z selected galaxies in Kodama et al. (2001). Therefore, our wide-field emission-line survey suggests the existence of a prominent structure traced by star-forming galaxies in the north direction of Abell 851. This new group (Group-1) is defined as a circle in Fig. 5. Finally, as a comparison, we define the three “Field” regions as indicated in Fig. 5, in which we avoid any prominent structures.

4.2. H α fraction

We here calculate the fraction of H α emitters for each environment defined above (see the labels in Fig. 6). We statistically subtract the expected contaminations in our phot- z based membership using the surface number density of the “Field” regions, $\rho_{cont} = 2.06 \text{ arcmin}^{-2}$. We calculate the H α fraction in each environment using the following equation:

$$f(\text{H}\alpha) = \frac{N_{\text{H}\alpha}}{N_{\text{member}} - N_{\text{cont}}}, \quad (4)$$

where $N_{\text{H}\alpha}$, N_{member} and N_{cont} represent the numbers of H α emitters, all member galaxies (phot- z members or H α emitters) and the expected contaminations (i.e. $N_{\text{cont}} = \rho_{\text{cont}} \times S$, where S is the surface area of each environment), respectively. In this calculation, we limit our sample to the galaxies with $z' \leq 23$ mag, since the selection of H α emitters becomes incomplete below this magnitude as can be seen in Fig. 3. In Fig. 6, filled circles with error bars indicate the values after the statistical subtraction, while open triangles show those be-

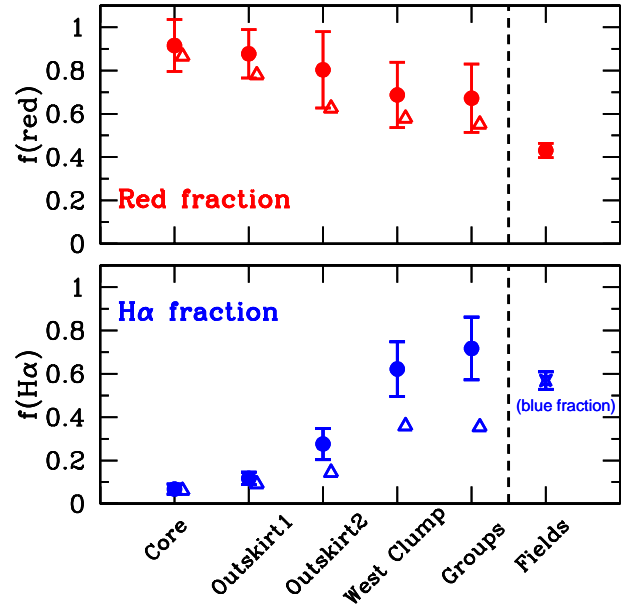


FIG. 6.— The H α fraction (bottom) and the red galaxy fraction (top) as a function of environment, calculated for the galaxies with $z' < 23$ mag. The open triangles and filled circles indicate the values before and after the statistical subtraction of the contaminant galaxies, respectively. The error bars present the Poissonian errors. For the field environment, we show only the red galaxy fraction before statistical correction and the blue galaxy fraction instead of H α fraction (see text).

fore subtraction. It can be seen that the H α fractions are almost unchanged after statistical subtraction in the dense cluster central region, while the contribution of contaminant galaxies gets larger in poorer environments. Note that, since we can not calculate the H α fraction for the field environment by definition (see equation 4), we present instead the blue galaxy fraction calculated based on the phot- z selected galaxies in the field environment as a rough estimate of the fraction of star forming galaxies. This assumption would be reasonable because we find that the fraction of H α emitter among blue galaxies is ~ 1 at all environments after statistical correction. However, as will be discussed in the next section, there must be H α emitters with red colors as well. Therefore, the blue galaxy fraction shown here for field environment may be a lower limit of the H α fraction. We also note that, although our “Field” environment avoids any prominent structures, it is still located near the rich clus-

ter. This may lead to an overestimation of contaminant galaxies in the above calculation. However, our results including the “relative” trends seen in Fig. 6 would not change even if we do not apply any correction for the contamination.

In Fig. 6, it is evident that the $H\alpha$ emitter fraction sharply declines toward the higher-density environment (only $\sim 10\%$ in the core and Outskirt-1, in contrast to $\gtrsim 50\%$ in the west clump and groups), suggesting the clear environmental dependence of star forming activity at $z \sim 0.4$. We also show the fraction of red galaxies with $B - I > 2$ in the top panel of Fig. 6 (again, open triangles and filled circles indicate before and after statistical subtraction). The trend of increasing fraction of red galaxies toward the cluster center is consistent with our result obtained from the analysis on the $H\alpha$ fraction (i.e. the bottom panel of Fig. 6).

It is now clear that the fraction of star forming galaxies is significantly lower in the cluster central regions than in the other surrounding environments (see also Sato & Martin 2006b for the measurements of [OII] emitter fraction within ~ 3 Mpc from the cluster), although some $H\alpha$ emitters are found in the core of Abell 851 (see Fig. 5 and Oemler et al. 2009). Such $H\alpha$ emitters found in the cluster central region are not distributed uniformly over the cluster environment but concentrated along the north-south direction near the core. In particular, we find a strong concentration of $H\alpha$ emitters at $\sim 1.5'$ north from the cluster center, and this position coincides with the “North group” noted by Oemler et al. (2009) where they also found a large number of star forming galaxies. Therefore, it may be possible that a part of the star forming galaxies found in the cluster central region belong to a group moving near the cluster central region in projection.

5. RED STAR FORMING GALAXIES

We have mapped out the spatial distribution of the $H\alpha$ emitters across the $\sim 30'$ field around Abell 851. The majority of the $H\alpha$ emitters have blue colors with $B - I \leq 2$. This is a natural consequence of young stellar populations in actively star forming galaxies. On the other hand, we have also identified a large number of red $H\alpha$ emitters throughout the field (red squares in Fig. 5). We here focus on the environment and nature of such red $H\alpha$ emitters, because they may be transitional galaxies migrating from the blue cloud to the red sequence.

5.1. Environment of red $H\alpha$ emitters

To examine the colors of the $H\alpha$ emitters and its environmental dependence in detail, we construct color-magnitude diagrams in Fig. 7. We divide the sample into five environmental bins as defined in the previous section, namely, cluster core, two cluster outskirts, west clump and groups (Group-1,2,3, and 4). We use the same color symbols as used in Fig. 5 (i.e. blue, green and red squares for normal, weak and red $H\alpha$ emitters, respectively). Fig. 7 shows the most important and impressive result of this paper. We find almost no red $H\alpha$ emitters in the central cluster regions (i.e. in the cluster core and the two outskirts regions). In contrast, we see a large number of red emitters in the west clump and in the groups. To quantify this, we calculate the fraction of red galaxies among all $H\alpha$ emitters in each environment (see

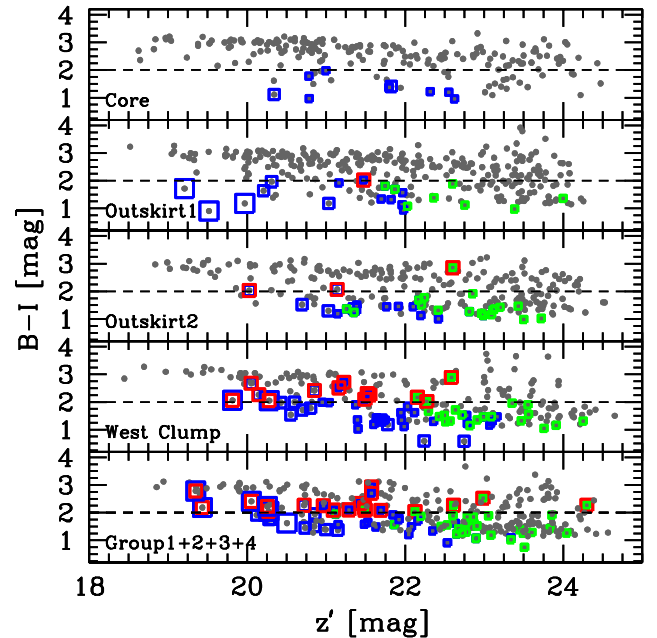


FIG. 7.— The color-magnitude diagram for each environment as indicated in each panel. The definition of the environment is shown in Fig. 5 and the meanings of the symbols are also the same as in Fig. 5. The horizontal dashed line at $B - I = 2$ is the dividing line between red and blue galaxies in this paper. It is clear that the red $H\alpha$ emitters are much more common in the group-scale environments.

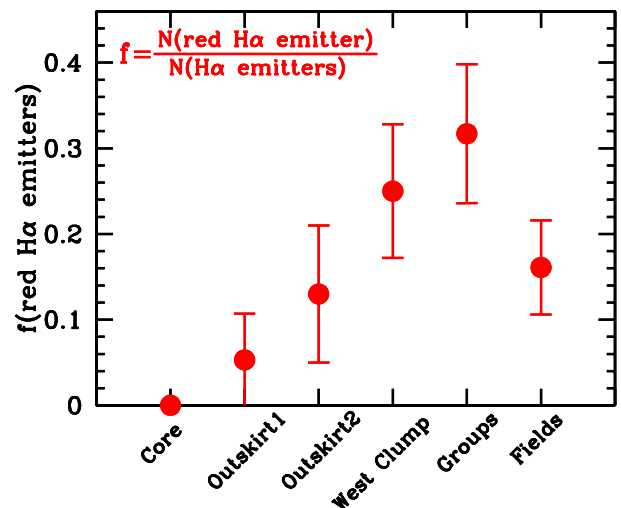


FIG. 8.— The fraction of red galaxies among all $H\alpha$ emitters with $z' < 23$ mag. A clear deficit of red $H\alpha$ emitters is seen in the cluster central regions. Note that only the $H\alpha$ emitters are used in this calculation, so that no statistical subtraction is needed. The error bars indicate Poissonian uncertainties.

Fig. 8). This plot clearly shows that the red $H\alpha$ emitters are seen exclusively in the relatively low-density environments. We find that a surprisingly high fraction ($\gtrsim 20$ – 30%) of $H\alpha$ emitters in the west clump or in the groups show red colors, which probably suggests that dusty star forming activities are triggered in such environments (see also discussion in Section 5.3).

Note that the definition of “red galaxies” here includes not only the galaxies on the red-sequence but also those in the “green-valley”. However, our result is not affected even if we select only the red-sequence galaxies, although the number of red $H\alpha$ emitters becomes smaller in this case. We combined the four groups to obtain a composite value for the group environment so that we can achieve better statistics, although we find that the fraction is nearly constant at $\sim 30\%$ in all the groups. It is also interesting to note that we find three red $H\alpha$ emitters in the Outskirt-2 region (see the middle panel of Fig. 7), but they are all located in the southern filament connecting the cluster core and the Group-2 (see Fig. 5). This may suggest that the galaxies falling into the cluster along the filamentary structure are experiencing somewhat different environmental effects from those for galaxies falling directly into the cluster from other various directions.

It is clear that the red $H\alpha$ emitters are absent in the cluster central region. We note that this deficit of red $H\alpha$ emitters does not simply reflect the environmental dependence of the color distribution of overall galaxy populations. As shown in the top panel of Fig. 6, the fraction of red galaxies monotonically increases toward the cluster center (equally, those $H\alpha$ emitters near the cluster core are almost exclusively blue). Therefore, the environmental trend of the red galaxies and that of the red $H\alpha$ emitters are clearly different, and so there is a clear difference in star forming activity between cluster and group/filament environments.

One may claim that the definitions of the groups and the west clump are somewhat arbitrarily chosen. In order to assess the effect of the uncertainty in the definition of environment, we apply another definition of environments, based on the local density of galaxies (i.e. Σ_{10th} using all the phot- z members). We then investigate the dependence of colors of $H\alpha$ emitters on the local density. The trends seen in Figs. 7 and 8 are still visible, but weaker. In fact, we find that the local densities of the Outskirt-2 and the groups are similar, but the occurrence of the red $H\alpha$ emitters is different (\sim twice larger in the groups than in the Outskirt-2, although the error-bars are large). This may suggest that star forming activity is determined not solely by local environment but also by global environment.

We should note that the preferred environment of the red $H\alpha$ emitters may change with redshift. In fact, we have shown in Koyama et al. (2010) that red $H\alpha$ emitters are located immediately outside of the cluster core at $z \sim 0.8$. However, our current analysis on Abell 851 suggests that at $z \sim 0.4$ red $H\alpha$ emitters are found in group environment relatively far away from the cluster, and that such galaxies are very rare even in the cluster outskirts. This may support the “propagation scenario” of star formation in clusters, that is, the site of the red star forming galaxies (probably the transition objects) shifts from cluster cores to outer regions from $z \sim 1.5$ to the present-day Universe (see also Hayashi et al. 2010). However, the situation might be more complicated, given that there exist heavily obscured mid-infrared (MIR) bright galaxies as well. A more detailed discussion including such MIR sources will follow in the next sections.

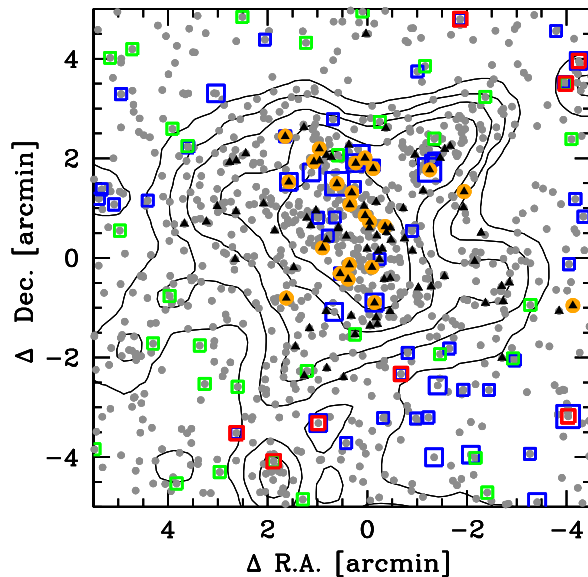


FIG. 9.— A close-up view of the cluster central region with the positions of MIPS-detected sources (orange circles). The meanings of the other symbols are the same as in Fig. 5, except for the black triangles which show the spectroscopic members within the MIPS data coverage, taken from Oemler et al. (2009).

5.2. Mid-infrared sources

The central $\sim 5' \times 5'$ region of Abell 851 was observed with Spitzer MIPS ($24\mu\text{m}$) by Dressler et al. (2009). They reported that some galaxies in the core of Abell 851 are detected in MIR. Here, we show in Fig. 9 the spatial distribution of such MIPS sources taken from the catalog in Oemler et al. (2009) overlaid on the distribution of our $H\alpha$ emitters. We only show the cluster central region due to the small coverage of the MIPS data. The MIPS sources are shown by orange circles. It is apparent that the spatial distribution of the $H\alpha$ emitters and the MIPS sources are qualitatively similar, and they are both concentrated in the north-south direction. In fact, some sources are directly overlapping each other. We also construct a color-magnitude diagram for the central region with $R_c < 1$ Mpc (Fig. 10). The MIPS sources are again shown by orange circles in Fig. 10. They are located on the slightly bluer side of the red sequence and also at the bright end of the “blue cloud” and the “green valley”. Some of the MIR galaxies are overlapping with $H\alpha$ emitters, but interestingly, most of the red MIR galaxies with $B - I > 2$ are *not* detected in $H\alpha$, although these MIPS sources are all spectroscopically confirmed members and many of them should have been detected as $H\alpha$ emitters judging from their spectroscopic redshifts (see below). Therefore, we should keep in mind that the lack of red $H\alpha$ emitters in the cluster central region does not necessarily mean the lack of “red star forming” galaxies there.

Dressler et al. (2009) examined the spectral type of MIPS-detected sources and found that many of the MIPS sources in Abell 851 have “e(a)-type” spectra (strong Balmer absorption *and* [OII] emission lines), which are interpreted as on-going dusty starbursts (e.g. Poggianti et al. 1999; Poggianti & Wu 2000).

TABLE 2
PROPERTIES OF SPECTROSCOPICALLY CONFIRMED MIPS SOURCES IN ABELL 851.

redshift	spectral type	$B - I$ [mag]	$EW_R(\text{H}\alpha + [\text{NII}])$ [Å]	$\text{SFR}(\text{H}\alpha)$ [M_\odot/yr]	$f_{24\mu\text{m}}$ [Jy]	$\text{SFR}(\text{IR})$ [M_\odot/yr]	$\text{H}\alpha$ emitter (yes/no)
0.4084	e(c)	1.11	34.52	3.51	3.05×10^{-4}	10.2	yes
0.4059	e(a)	1.78	29.04	1.98	1.63×10^{-4}	5.0	yes
0.3972	e(n)	0.75	147.31	22.93	7.96×10^{-4}	30.1	yes
0.4010	e(a)	1.92	30.84	1.48	1.30×10^{-4}	3.8	yes
0.3958	e(b)	0.91	145.75	27.45	1.04×10^{-3}	40.3	yes
0.3932	e(a)	1.64	28.90	3.35	2.12×10^{-4}	6.8	yes
0.4061	e(n)	1.72	69.79	19.24	3.98×10^{-3}	165.5	yes
0.3937	e(a)	1.97	38.64	4.02	4.82×10^{-4}	17.2	yes
0.4007	k+a	2.70	8.66	4.44	5.21×10^{-4}	18.7	no
0.4060	k+a	2.36	3.59	1.82	3.14×10^{-4}	10.6	no
0.4075	a+k	2.30	-2.57	-0.37	1.12×10^{-4}	3.2	no
0.4076	e(a)	1.65	21.00	0.59	8.13×10^{-5}	2.2	no
0.3938	k+a	2.30	14.27	3.69	5.78×10^{-4}	21.1	no
0.4083	k+a	2.50	0.91	0.10	1.49×10^{-4}	4.5	no
0.3960	k	2.84	0.40	0.07	7.32×10^{-4}	27.4	no
0.4017	k	3.17	-0.50	-0.04	1.01×10^{-4}	2.9	no

NOTE. — All the galaxies listed here are spectroscopically confirmed MIPS-detected members at $0.389 \leq z_{\text{spec}} \leq 0.409$ (i.e. $\text{H}\alpha$ lines of these sources fall within the FWHM of the NB921 filter), with spectral quality $Q \leq 3$ in Oemler et al. (2009). Remarkably, the MIPS sources without $\text{H}\alpha$ emissions (lower side) tend to be redder and to have spectral types without emission lines (i.e. k/k+a/a+k) compared to those with $\text{H}\alpha$ detections (upper side). Redshifts, spectral types and $f_{24\mu\text{m}}$ are taken from Oemler et al. (2009). In deriving $\text{SFR}(\text{IR})$, we first estimate $L(\text{IR})$ by using the SED templates of starburst galaxies in Lagache et al. (2004) and then convert it to $\text{SFR}(\text{IR})$ based on the Kennicutt (1998) calibration. Two sources have negative values of $EW(\text{H}\alpha + [\text{NII}])$ and $\text{SFR}(\text{H}\alpha)$ due to their negative (but almost ~ 0) $z' - \text{NB921}$ colors.

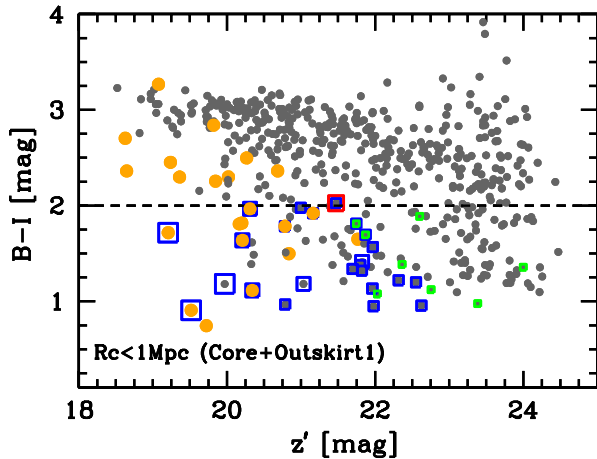


FIG. 10.— A color-magnitude diagram for the cluster central region ($R_c < 1\text{Mpc}$). The meanings of the symbols are the same as in Fig. 9. MIPS sources are again shown by orange filled circles.

Dressler et al. (2009) also noted that a significant fraction ($\sim 30\%$) of “k+a” or “a+k” galaxies (strong Balmer absorption *without* $[\text{OII}]$ emission lines), which are often interpreted as *post-starburst* galaxies, are detected in MIR (see also Smail et al. 1999 for the radio continuum detection with VLA from k+a galaxies in the Abell 851). In the spectroscopic catalog of Abell 851 in Oemler et al. (2009), 22 galaxies with $Q \leq 3$ are detected with MIPS (i.e. $f_{24\mu\text{m}} \geq 80\mu\text{Jy}$ or $\text{SFR}_{\text{IR}} \gtrsim 3M_\odot/\text{yr}$). We find that 6 out of these 22 sources have redshifts slightly outside of our $\text{H}\alpha$ survey (their $\text{H}\alpha$ lines fall outside of the FWHM of the NB filter), but we can expect to detect $\text{H}\alpha$ emission from the remaining 16 sources. However, we find that only 8 galaxies (50%) satisfy our $\text{H}\alpha$ emitter selection criteria, while the remaining 8 galaxies (50%)

are not detected in $\text{H}\alpha$ (see Table 2). These galaxies are likely to be heavily attenuated by dust, so that even the $\text{H}\alpha$ emission cannot come through. Furthermore, we find a systematic difference in spectral types between $\text{H}\alpha$ -detected and $\text{H}\alpha$ -undetected MIPS sources (again, see Table 2). All the $\text{H}\alpha$ -detected MIPS sources show “e(a,b,c,n)” spectra (i.e. $[\text{OII}]$ emission lines are present in their spectra), while many of the $\text{H}\alpha$ -undetected MIPS sources show “k+a/a+k” spectra (or “k”-type in two cases) without $[\text{OII}]$ emission lines. We can also confirm in Table 2 that the $\text{H}\alpha$ -undetected MIPS sources have systematically redder colors than the $\text{H}\alpha$ -detected ones ($\langle B-I \rangle = 1.48$ and 2.48 for $\text{H}\alpha$ -detected and $\text{H}\alpha$ -undetected objects, respectively). These results suggest that some red galaxies do not show $\text{H}\alpha$ or $[\text{OII}]$ emission lines in spite of their significant amount of hidden star formation activities.

5.3. What are the red $\text{H}\alpha$ emitters ?

It is naturally expected that star forming galaxies show blue colors because young, massive, hot stars dominate their total light. Therefore, the interpretation for the red galaxies with emission lines is not straightforward. The most likely interpretation for the red $\text{H}\alpha$ emitters is that they are *dusty red galaxies* (e.g. Wolf et al. 2005; 2009). If a star forming galaxy contains a significant amount of dust, it appears red due to the selective extinction of bluer light, and in some cases, it becomes difficult to be distinguished from passively evolving red galaxies. Furthermore, in the extremely dusty cases, even the $\text{H}\alpha$ lines are heavily attenuated by dust and large corrections are required to obtain true star formation rates from the observed $\text{H}\alpha$ intensities (e.g. Poggianti & Wu 2000). This may explain the fact presented in the previous subsection that optically red MIPS-detected galaxies in the Abell 851 do not show significant $\text{H}\alpha$ emissions.

An important point here is that, in contrast to the fact that the optically red MIPS sources in the cluster core are not detected in $H\alpha$, we do find many red $H\alpha$ emitters in the group environments. If there are similar MIR-bright dusty red sources in groups, they should *not* have been detected in $H\alpha$ in the groups, either. Why do only the red star forming galaxies in groups have detectable $H\alpha$ emissions? A possible answer would be: (1) the star formation rates of these galaxies in groups are significantly higher and have stronger intrinsic $H\alpha$ intensities, and/or (2) the mode of star formation in these systems is different from the MIPS sources in the cluster core (e.g. the location of star formation within galaxies and/or the geometry of dust extinction would be different).

5.3.1. *Strong starbursts or moderate star formation ?*

It has been reported that there is an excess of IR luminous star forming galaxies in group-like environments in the distant Universe. For example, Tran et al. (2009) studied a supergroup environment at $z \sim 0.4$ in the MIR and showed an excess at the bright end of the IR luminosity function in group environment compared to cluster/field environments. Also, Poggianti et al. (2009) studied the spectra of galaxies in the EDisCS clusters at $z = 0.4-0.8$ and showed that the “e(a)-type” galaxies (those having a signature of dusty starburst in their optical spectra) are most numerous in group environments. This excess in star forming activity of group galaxies may suggest that galaxy transition is actively taking place in group environments, and some galaxies with exceptionally high SFR may be detected in $H\alpha$. Also, recent MIR studies of distant clusters at $z \gtrsim 0.5$ found a large number of luminous infrared galaxies (LIRGs) in the outskirts of clusters (e.g. Marcillac et al. 2007; Koyama et al. 2008), and so it is likely that such dusty starburst galaxies are included in our red $H\alpha$ emitter sample. In fact, Koyama et al. (2010) discovered some red $H\alpha$ emitters in the outskirts of a $z = 0.81$ cluster, and found that most of these red $H\alpha$ emitters are indeed MIR-detected LIRGs with significant extinction at $H\alpha$ ($A_{H\alpha} \gtrsim 3$ mag). Geach et al. (2009) conducted MIR spectroscopy for some LIRGs in the outskirts of the CL0024 cluster at $z = 0.4$ reported in Geach et al. (2006). They identified clear PAH emission features from the majority of their targets, suggesting that these LIRGs are really dusty starbursts (AGN contribution is small). Their MIR spectra resemble those of nuclear starbursts rather than normal star formation in disks, and they proposed that such dusty starbursts seen in the outskirts of distant clusters are progenitors of the present-day cluster S0 galaxies (see also the discussion in Section 5.3.2).

However, such extremely active galaxies tend to be more dusty, and it might be difficult to detect their $H\alpha$ emission. Also, the time-scale of dusty starbursts is not long, typically $\lesssim 1$ Gyr. In our sample, we detect $H\alpha$ emission for $\sim 20-30\%$ of the red galaxies in the west clump and in the groups. This fraction may be too large, if we assume that they are *all* short-lived dusty starbursts. It is more likely that a gentle mechanism which produces relatively long-lived red star forming galaxies is also at work in the group environment around the Abell 851 cluster. Wolf et al. (2009) studied dusty red galaxies in the complex structure of the Abell 901/902 clus-

ters at $z = 0.17$ with UV+MIR photometry, and found that their specific SFRs are systematically lower than blue star forming galaxies (see also Wolf et al. 2005 and Gallazzi et al. 2009 for their identification of dusty red galaxies). They concluded that the dusty red galaxies in Abell 901/902 are “semi-passive” rather than intense starbursts. They also proposed that the origin of such red star forming galaxies is similar to that of “passive spirals” (galaxies with spiral morphology but without ongoing star formation activity; e.g. Poggianti et al. 1999, Goto et al. 2003). Although a direct comparison of their results with ours is difficult, a fraction of the red $H\alpha$ emitters identified in our survey could be similar to the dusty red galaxies discussed in Wolf et al. (2009) which are not strongly star-bursting galaxies but moderately star-forming dusty galaxies.

5.3.2. *Progenitors of the cluster S0 galaxies ?*

The existence of a large number of red star forming galaxies and their location (i.e. preferably in groups) may indicate that such populations are highly related to the transformation of galaxies due to environmental effects, as there is a hint that the group environment is a key place for galaxy truncation and the formation of S0 galaxies (see e.g. Wilman et al. 2008; 2009). It has been reported that the fraction of S0 galaxies in cluster cores dramatically increases from $z \sim 0.5$ to $z \sim 0$ (e.g. Dressler et al. 1997; Desai et al. 2007; Poggianti et al. 2009; Just et al. 2010), and it has been widely discussed in terms of the transformation from infalling field spirals to cluster S0s as they assemble to clusters (e.g. Poggianti et al. 1999; Kodama & Smail 2001). To reconstruct the S0 fraction in the nearby clusters, it may be required that galaxies are “pre-processed” in group environments (e.g. Fujita 2004), and late-type spirals (S_{cdm}) may be transformed into bulge-strong early spirals such as S_{ab} in the group environment (Kodama & Smail 2001). Moreover, considering the high bulge-to-disk ratios of S0 galaxies, just a simple fading of spiral disks may not be sufficient to produce S0 galaxies (Christlein & Zabludoff 2004). The physical processes which can move the gas toward the galaxy center and can grow their bulges through a new star formation activity would be preferable. The galaxy-galaxy interactions or harassment expected in groups are the best candidates (see also the discussion in Moran et al. 2007). In this context, many of the red $H\alpha$ emitters reported in this paper may be in the phase of growing bulges with significant star formation in the galactic central regions with moderate dust extinction. However, the star formation activity is not as strong as a starburst, and their $H\alpha$ emission is still visible through moderate dust extinction.

Moran et al. (2007) studied passive spirals and young S0 galaxies in two clusters at $z = 0.4$ and 0.5 . They found that these transitional objects are preferentially seen in the infalling groups, and they also found that some of them are detected in UV. Such galaxies are probably similar populations to our red $H\alpha$ emitters. Moran et al. (2007) also examined the UV/optical colors of these objects and proposed that they are likely to be truncated with a long time-scale ($\gtrsim 1$ Gyr), qualitatively consistent with our suggestion of long time-scales of the red $H\alpha$ emitters in group environment. On the other hand, Moran et al. (2007) found that the star for-

mation is more rapidly truncated in the cluster core environment (especially for more massive cluster with strong ICM). In our analysis, we did not find red $H\alpha$ emitters in the cluster central region. This may be because the Abell 851 cluster is also a very rich cluster, and possibly red $H\alpha$ emitters cannot survive in the strong ICM in the cluster core (maybe their star formation is immediately shut off after entering the cluster core). In contrast, the MIPS-detected galaxies found in the cluster central region would be more intense short-lived starbursts with stronger extinction, probably triggered by galaxy mergers as suggested by Oemler et al. (2009).

Unfortunately, we do not have MIR data (which are essential for identifying obscured starbursts) and high-resolution HST data (which are also essential to resolve galaxy morphology, mergers and localized star formation) for the group environments where we find a large number of red $H\alpha$ emitters. These information should be powerful for understanding the physical origin of the pre-processing working in the group environment, which may be closely related to the formation of cluster S0 galaxies. Combining these data with our wide-field $H\alpha$ imaging data will be clearly an important future work.

5.3.3. Summary

In summary, the red $H\alpha$ emitters are most commonly seen in galaxy groups around Abell 851. They are probably related to the physics of the “pre-processing” in group environments forming cluster S0 galaxies prior to entering the cluster core. The physical mechanisms mainly responsible for these populations are likely to be group-specific slow processes such as strangulation (e.g. Larson et al. 1980; Bekki et al. 2002; Kawata & Mulchaey 2008) or harassment-like mechanisms (e.g. Moore et al. 1999; Moran et al. 2007). The latter might be more preferred if they are in the process of morphological change toward the more bulge-dominated early spirals at the same time. Strong dusty starbursts triggered by e.g. galaxy-galaxy interactions or mergers may also be included in our red $H\alpha$ emitter sample, as we actually found such a population in the study of the $z \sim 0.8$ cluster (see Koyama et al. 2010). However, it is currently difficult to quantify their relative contribution or its redshift evolution. The most demanding and promising next step is a wide-field observation of the infalling groups in the MIR/FIR with the future space IR missions. Dusty starbursts should be bright in IR, while gradually fading star forming galaxies would not be so bright in IR. Such surveys will give us a critical information to identify the key process for the evolution of cluster galaxies.

6. CLUSTER TOTAL STAR FORMATION RATE

Our narrow-band $H\alpha$ line survey is also capable to study total star formation rate in clusters. The advantage of the narrow-band survey is that we can trace star forming activity throughout the observed field, and that we do not suffer from a sample selection bias or a completeness correction, which are inevitable for slit spectroscopy. The wavelength range of the narrow-band filter used in this study is slightly offset from the actual redshift distribution of the cluster member galaxies in $H\alpha$ (see Fig. 1). We correct for it in a statistical manner. We use the velocity distribution of the spectroscopic

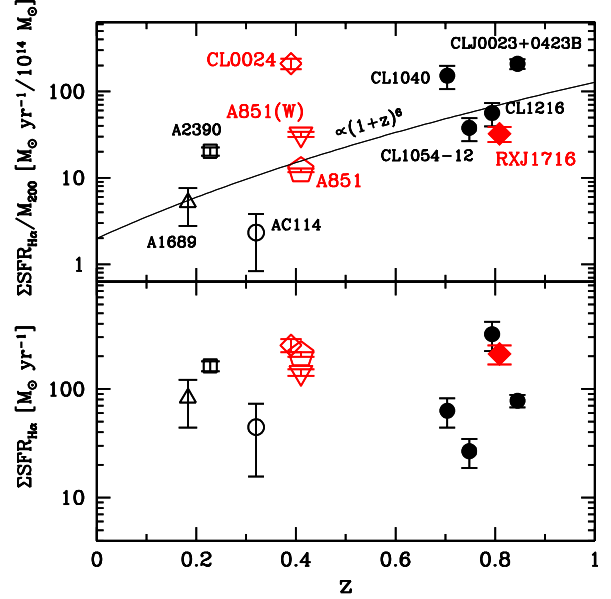


FIG. 11.— (bottom): The integrated total SFR($H\alpha$) within $0.5 \times R_{200}$ as a function of redshift. Our measurements based on the Subaru data including our previous surveys are shown by red symbols. (top): The integrated total SFR($H\alpha$) normalized by the cluster mass M_{200} as a function of redshift.

members within $0.5 \times R_{200}$ from Oemler et al. (2009), and estimate the fraction of $H\alpha$ emission from the Abell 851 cluster that can be recovered by our NB921 filter. The resultant correction factor to get the total star formation rate turns out to be $\sim 1.54^{+0.08}_{-0.06}$ (the uncertainty is given as a 1σ deviation derived from a bootstrap resampling of the spectroscopic members).

Following the procedure in Finn et al. (2005) and Koyama et al. (2010), we sum up the star formation rates of $H\alpha$ emitters within $0.5 \times R_{200}$ from the cluster center to derive $\Sigma SFR_{H\alpha}$, where R_{200} is the radius within which the mean density is 200 times larger than the critical density of the Universe (Carlberg et al. 1997). This allows us to directly compare our data with previous $H\alpha$ -based cluster studies over a wide range in redshift, which have been compiled by Finn et al. (2005). We also calculate the cluster mass, M_{200} , as in Koyama et al. (2010) and derive the cluster mass-normalized star formation rate (i.e. $\Sigma SFR_{H\alpha}/M_{200}$). The R_{200} and M_{200} are calculated in the following equations:

$$R_{200} = 2.47 \times \frac{\sigma}{1000 \text{ km/s}} \frac{1}{\sqrt{\Omega_{\Lambda} + \Omega_{\text{M}}(1+z)^3}} \text{ Mpc} \quad (5)$$

$$M_{200} = 1.71 \times 10^{15} \left(\frac{\sigma}{1000 \text{ km/s}} \right)^3 \frac{1}{\sqrt{\Omega_{\Lambda} + \Omega_{\text{M}}(1+z)^3}} M_{\odot}, \quad (6)$$

where σ is the velocity dispersion of the cluster. Using the velocity dispersion of the cluster core galaxies ($\sigma = 1071 \text{ km/s}$; Oemler et al. 2009) and the cosmological parameters adopted in this paper, we derived $R_{200} = 2.13 \text{ Mpc}$ and $M_{200} = 1.70 \times 10^{15} M_{\odot}$. Then, using all galaxies with $z' - \text{NB921} > 3\sigma$, we derived $\Sigma SFR_{H\alpha} = 208 \pm 10 M_{\odot}/\text{yr}$ and the mass-normalized star formation rate of $\Sigma SFR_{H\alpha}/M_{200} = 12.2 \pm 0.6 M_{\odot} \text{ yr}^{-1}/10^{14} M_{\odot}$.

These values include the correction for the filter transmission curve as described above (i.e. a factor of ~ 1.5), and the error-bars are given as a composite of the photometric errors and the uncertainty of the correction factor.

Note that we include all galaxies with $z' - \text{NB921} > 3\sigma$ that satisfy the same color selection criteria as in Fig. 3. If we use only the secure H α emitters as defined in this study (i.e. $z' - \text{NB921} > 3\sigma$ and $z' - \text{NB921} > 0.2$), these values would become smaller by a factor of ~ 2 (lower limit), and if we use all galaxies with $z' - \text{NB921} > 0$, these values would increase by $\sim 25\%$ (upper limit). Although this uncertainty is large, this does not affect our main conclusion. We expect that the uncertainty regarding the dust extinction may also be very large. In fact, we derive $\Sigma \text{SFR}(\text{IR}) \sim 370 M_\odot/\text{yr}$ by just summing up the IR-derived SFRs of the 16 MIPS-detected spec- z members listed in Table 2, which is clearly larger than $\Sigma \text{SFR}(\text{H}\alpha)$ derived above. Although we use a constant 1 mag extinction correction in this paper to make a fair comparison with the values in other works in the literature, it is also essential to study such obscured/hidden activities more in detail with the MIR–FIR observations (see some examples of such IR studies of the global evolution of star forming activities in clusters by e.g. Geach et al. 2006; Bai et al. 2007; Koyama et al. 2010; Haines et al. 2009a; Chung et al. 2011).

We plot in Fig. 11 the values derived above and compare them with those for other clusters in the literature all based on H α (see Koyama et al. 2010 and references therein). This plot clearly shows that the mass-normalized star formation rate of Abell 851 is located on the general evolutionary trend with redshift, following approximately $\propto (1+z)^6$. The lower limit in SFR that is used to calculate ΣSFR is slightly different from cluster to cluster, but it is within the range of $0.1\text{--}1 M_\odot/\text{yr}$ (dust-free). Since the integrated SFRs are dominated by galaxies with strong star formation, we do not correct for this effect (see also Finn et al. 2004; Kodama et al. 2004). The strong evolution of star forming activity in clusters presented above is well consistent with our previous study in Koyama et al. (2010), and this trend is much more significant than the trend of a decrease in the specific star formation rates of *individual* galaxies, $\propto (1+z)^3$ shown by e.g. Yoshida et al. (2006); Zheng et al. (2007) (see also the H α -based studies of cosmic star formation history by e.g. Sobral et al. 2009; Westra et al. 2010; Dale et al. 2010). Therefore, our result also suggests that cluster environment does indeed accelerate the quenching of activities in galaxies.

We note that this redshift dependence of the cluster mass-normalized star formation rates (or its scatter) may be related to the cluster mass growth (e.g. Finn et al. 2005; Koyama et al. 2010). As presented in Koyama et al. (2010), more massive clusters exhibit lower $\Sigma \text{SFR}_{\text{H}\alpha}/M_{200}$ (see also Homeier et al. 2005; Bai et al. 2009). This may also be related to the fact that the fraction of star forming galaxies is a decreasing function of cluster mass (e.g. Poggianti et al. 2006, but see a different result by Haines et al. 2009). In fact, a large scatter between clusters is clearly visible even at a fixed redshift in the top panel of Fig. 11. In particular, the value of Abell 851 presented in this paper is significantly different from that of CL0024 cluster at a similar redshift (see Fig. 11). However, Abell 851 is ~ 1 order of magni-

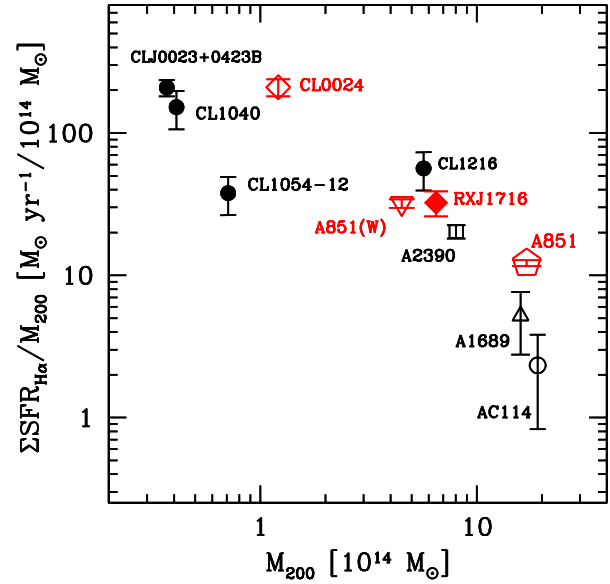


FIG. 12.— The integrated total SFR(H α) normalized by the cluster mass as a function of cluster mass, M_{200} . The symbols are the same as Fig. 11. Open and filled symbols indicate the low- z samples ($z \lesssim 0.4$) and the high- z samples ($z \gtrsim 0.6$), respectively.

tude more massive than CL0024, and both clusters still lie along the general trend of decreasing $\Sigma \text{SFR}_{\text{H}\alpha}/M_{200}$ with increasing cluster mass (Fig. 12). Furthermore, we also calculated these values for the West Clump of Abell 851 in the same way as for the main cluster, adopting the R_{200} and M_{200} taken from the preliminary result of the optical spectroscopy by Nakata et al. (2011). We plotted these values for the west clump in Figs. 11 and 12. Interestingly, the west clump of Abell 851 is more massive than CL0024 cluster and has a lower value of $\Sigma \text{SFR}_{\text{H}\alpha}/M_{200}$, indicating the importance of the mass of the structure in determining the star forming activity in the system.

We should comment that this simultaneous trend of ΣSFR vs. cluster mass and ΣSFR vs. redshift makes it difficult to derive any evolutionary trend in star formation activities in clusters. Our fitting of a form $\Sigma \text{SFR} \propto (1+z)^m \times M_{\text{cl}}^n$ to the data shown in Figs 11 and 12 yielded $m = 1.2 \pm 2.0$ and $n = -0.75 \pm 0.2$. However, these numbers should be taken as very preliminary because they are based on a small sample. It should be also noted that, as shown in Fig. 12, the low- z clusters (open symbols) studied so far tend to be more massive, while the high- z clusters (filled symbols) tend to be less massive. This may have led to an apparently stronger evolutionary trend than the actual one. It is thus critically important to collect a large number of distant clusters covering various masses and redshifts with future large cluster surveys.

7. SUMMARY AND CONCLUSIONS

We performed a panoramic narrow-band H α emitter survey for an intermediate redshift cluster Abell 851 at $z = 0.41$ with Suprime-Cam on the Subaru Telescope. This is one of the most distant wide-field H α emitter surveys ever made for clusters. After selecting the H α

emitters with color excess in z' -NB921 and the broad-band color information, we first map out the spatial distribution of the H α emitters around Abell 851. The H α emitters are found throughout the observed $27' \times 27'$ field, suggesting that the large-scale structures identified by our previous optical imaging survey are really located at the cluster redshift and physically associated with the main cluster. The fraction of H α emitters is a strong function of environment and shows a clear decline toward the cluster central region.

The most important result of this study is the color variation of H α emitters and its clear environmental dependence. The majority of the H α emitters are blue galaxies with $B - I < 2$, but we find that $\sim 15\%$ of the H α emitters have red colors. Such red H α emitters are preferentially found in the group environment relatively far away from the cluster core. Our survey shows that ~ 20 – 30% of H α emitters in the west clump and the groups have red colors with $B - I > 2$, while such red emitters are very rare in and immediately outside of the cluster core ($\lesssim 5\%$). Some of the red H α emitters might be dusty starbursts with significant star formation produced via e.g. galaxy-galaxy interactions or mergers. However, it would be unlikely that *all* the red H α emitters are dusty starbursts, because most of the optically red MIR-detected galaxies found in the cluster central region are *not* detected in H α (and also because the number of red H α emitters is apparently too large for their expected short life time). Therefore, it would be reasonable to interpret that the red H α emitters in group environment are generated by relatively gentle and slow processes which are different from those producing MIR sources in the core of Abell 851. Also, a large number of the red H α emitters found in the groups might be closely related to the “pre-processing” contributing

to the formation of bulge-dominated cluster S0 galaxies before entering the cluster core region.

We also derived the cluster total star formation rate and the cluster mass-normalized star formation rate by summing up the star formation rates of individual galaxies within $0.5 \times R_{200}$ of the main cluster and the west clump. We confirmed a general trend that the mass-normalized star formation rates increase sharply toward distant clusters following approximately $\propto (1+z)^6$, which turned out to be remarkably consistent with our previous studies, although there is a large scatter between clusters. This scatter may be related to the variation of the cluster mass at each epoch. More massive clusters have lower star formation activity inside them, suggesting that the cluster mass growth is related to the suppression of the star formation activity in galaxies.

We thank the anonymous referee for relevant comments and suggestions. Y.K. also thank Dr. Kentaro Motohara, Prof. Kotaro Kohno, Prof. Masanori Iye, Prof. Yuzuru Yoshii, and Prof. Nobuo Arimoto for their careful reading of the manuscript and helpful comments. The broad-band and narrow-band imaging data used in this paper are collected at the Subaru Telescope, which is operated by the National Astronomical Observatory of Japan (NAOJ). Y.K. acknowledge the support from the Japan Society for the Promotion of Science (JSPS) through JSPS research fellowships for Young Scientists. This work was financially supported in part by a Grant-in-Aid for the Scientific Research (Nos. 18684004; 21340045) by the Japanese Ministry of Education, Culture, Sports and Science.

Facilities: Subaru .

REFERENCES

- Bai, L., et al. 2007, ApJ, 664, 181
 Bai, L., Rieke, G. H., Rieke, M. J., Christlein, D., & Zabludoff, A. I. 2009, ApJ, 693, 1840
 Bekki, K., Couch, W. J., & Shioya, Y. 2002, ApJ, 577, 651
 Belloni, P., Bruzual, A. G., Thimm, G. J., & Roser, H.-J. 1995, A&A, 297, 61
 Bertin, E., & Arnouts, S. 1996, A&AS, 117, 393
 Boselli, A., Gavazzi, G., Donas, J., & Scodreggio, M. 2001, AJ, 121, 753
 Brand, K., et al. 2009, ApJ, 693, 340
 Buson, L. M., Bertola, F., Cappellari, M., Chiosi, C., Dressler, A., & Oemler, A., Jr. 2000, ApJ, 531, 684
 Calzetti, D., Armus, L., Bohlin, R. C., Kinney, A. L., Koornneef, J., & Storch-Bergmann, T. 2000, ApJ, 533, 682
 Carlberg, R. G., Yee, H. K. C., & Ellingson, E. 1997, ApJ, 478, 462
 Christlein, D., & Zabludoff, A. I. 2004, ApJ, 616, 192
 Cowie, L. L., Barger, A. J., & Kneib, J.-P. 2002, AJ, 123, 2197
 Dale, D. A., et al. 2010, ApJ, 712, L189
 Davoodi, P., et al. 2006, MNRAS, 371, 1113
 De Filippis, E., Schindler, S., & Castillo-Morales, A. 2003, A&A, 404, 63
 Desai, V., et al. 2007, ApJ, 660, 1151
 Dressler, A., Rigby, J., Oemler, A., Fritz, J., Poggianti, B. M., Rieke, G., & Bai, L. 2009, ApJ, 693, 140
 Dressler, A., Smail, I., Poggianti, B. M., Butcher, H., Couch, W. J., Ellis, R. S., & Oemler, A., Jr. 1999, ApJS, 122, 51
 Dressler, A., et al. 1997, ApJ, 490, 577
 Dressler, A., Oemler, A., Jr., Sparks, W. B., & Lucas, R. A. 1994, ApJ, 435, L23
 Dressler, A., Oemler, A., Jr., Butcher, H. R., & Gunn, J. E. 1994, ApJ, 430, 107
 Dressler, A., & Gunn, J. E. 1992, ApJS, 78, 1
 Dressler, A. 1980, ApJ, 236, 351
 Finn, R. A., et al. 2005, ApJ, 630, 206
 Finn, R. A., Zaritsky, D., & McCarthy, D. W., Jr. 2004, ApJ, 604, 141
 Fujita, Y. 2004, PASJ, 56, 29
 Gallazzi, A., et al. 2009, ApJ, 690, 1883
 Garn, T., et al. 2010, MNRAS, 402, 2017
 Geach, J. E., Smail, I., Moran, S. M., Treu, T., & Ellis, R. S. 2009, ApJ, 691, 783
 Geach, J. E., et al. 2006, ApJ, 649, 661
 Gómez, P. L., et al. 2003, ApJ, 584, 210
 Goto, T., et al. 2003, PASJ, 55, 757
 Haines, C. P., et al. 2009, ApJ, 704, 126
 Haines, C. P., Smith, G. P., Egami, E., Okabe, N., Takada, M., Ellis, R. S., Moran, S. M., & Umetsu, K. 2009, MNRAS, 396, 1297
 Haines, C. P., Gargiulo, A., & Merluzzi, P. 2008, MNRAS, 385, 1201
 Hayashi, M., Kodama, T., Koyama, Y., Tadaki, K., & Tanaka, I. 2011, MNRAS, in press, arXiv:1104.2121
 Hayashi, M., Kodama, T., Koyama, Y., Tanaka, I., Shimasaku, K., & Okamura, S. 2010, MNRAS, 402, 1980
 Homeier, N. L., et al. 2005, ApJ, 621, 651
 Ichikawa, T., et al. 2006, Proc. SPIE, 6269,
 Iye, M., et al. 2004, PASJ, 56, 381
 Iye, M., et al. 2000, PASJ, 52, 9
 Just, D. W., Zaritsky, D., Sand, D. J., Desai, V., & Rudnick, G. 2010, ApJ, 711, 192

- Kawata, D., & Mulchaey, J. S. 2008, *ApJ*, 672, L103
- Kennicutt, R. C., Jr., & Kent, S. M. 1983, *AJ*, 88, 1094
- Kennicutt, R. C., Jr. 1992, *ApJ*, 388, 310
- Kennicutt, R. C., Jr. 1998, *ARA&A*, 36, 189
- Kennicutt, R. C., Jr., Lee, J. C., Funes, S. J., José G., Sakai, S., & Akiyama, S. 2008, *ApJS*, 178, 247
- Kodama, T., et al. 2005, *PASJ*, 57, 309
- Kodama, T., Balogh, M. L., Smail, I., Bower, R. G., & Nakata, F. 2004, *MNRAS*, 354, 1103
- Kodama, T., Smail, I., Nakata, F., Okamura, S., & Bower, R. G. 2001, *ApJ*, 562, L9
- Kodama, T., & Smail, I. 2001, *MNRAS*, 326, 637
- Kodama, T., Bell, E. F., & Bower, R. G. 1999, *MNRAS*, 302, 152
- Koyama, Y., Kodama, T., Shimasaku, K., Hayashi, M., Okamura, S., Tanaka, I., & Tokoku, C. 2010, *MNRAS*, 403, 1611
- Koyama, Y., et al. 2008, *MNRAS*, 391, 1758
- Koyama, Y., Kodama, T., Tanaka, M., Shimasaku, K., & Okamura, S. 2007, *MNRAS*, 382, 1719
- Larson, R. B., Tinsley, B. M., & Caldwell, C. N. 1980, *ApJ*, 237, 692
- Lagache, G., et al. 2004, *ApJS*, 154, 112
- Lewis, I., et al. 2002, *MNRAS*, 334, 673
- Mahajan, S., & Raychaudhury, S. 2009, *MNRAS*, 400, 687
- Marcillac, D., Rigby, J. R., Rieke, G. H., & Kelly, D. M. 2007, *ApJ*, 654, 825
- Martin, C. L., Lotz, J., & Ferguson, H. C. 2000, *ApJ*, 543, 97
- Miyazaki, S., et al. 2002, *PASJ*, 54, 833
- Moore, B., Lake, G., Quinn, T., & Stadel, J. 1999, *MNRAS*, 304, 465
- Moore, C. A., et al. 2010, *AJ*, 140, 253
- Moran, S. M., Ellis, R. S., Treu, T., Smith, G. P., Rich, R. M., & Smail, I. 2007, *ApJ*, 671, 1503
- Nakata, F., et al. 2011, in prep.
- Nakata, F., et al. 2005, *MNRAS*, 357, 1357
- Oemler, A., Dressler, A., Kelson, D., Rigby, J., Poggianti, B. M., Fritz, J., Morrison, G., & Smail, I. 2009, *ApJ*, 693, 152
- Ouchi, M., et al. 2004, *ApJ*, 611, 660
- Poggianti, B. M., et al. 2009, *ApJ*, 697, L137
- Poggianti, B. M., et al. 2009, *ApJ*, 693, 112
- Poggianti, B. M., et al. 2006, *ApJ*, 642, 188
- Poggianti, B. M., & Wu, H. 2000, *ApJ*, 529, 157
- Poggianti, B. M., Smail, I., Dressler, A., Couch, W. J., Barger, A. J., Butcher, H., Ellis, R. S., & Oemler, A., Jr. 1999, *ApJ*, 518, 576
- Salpeter, E. E. 1955, *ApJ*, 121, 161
- Sato, T., & Martin, C. L. 2006, *ApJ*, 647, 946
- Sato, T., & Martin, C. L. 2006, *ApJ*, 647, 934
- Schindler, S., Belloni, P., Ikebe, Y., Hattori, M., Wambsganss, J., & Tanaka, Y. 1998, *A&A*, 338, 843
- Schindler, S., & Wambsganss, J. 1996, *A&A*, 313, 113
- Smail, I., Morrison, G., Gray, M. E., Owen, F. N., Ivison, R. J., Kneib, J.-P., & Ellis, R. S. 1999, *ApJ*, 525, 609
- Smail, I., Dressler, A., Couch, W. J., Ellis, R. S., Oemler, A., Jr., Butcher, H., & Sharples, R. M. 1997, *ApJS*, 110, 213
- Sobral, D., Best, P. N., Smail, I., Geach, J. E., Cirasuolo, M., Garn, T., & Dalton, G. B. 2011, *MNRAS*, 411, 675
- Sobral, D., et al. 2009, *MNRAS*, 398, 75
- Springel, V., et al. 2005, *Nature*, 435, 629
- Stanford, S. A., Eisenhardt, P. R. M., & Dickinson, M. 1995, *ApJ*, 450, 512
- Suzuki, R., et al. 2008, *PASJ*, 60, 1347
- Tanaka, M., Lidman, C., Bower, R. G., Demarco, R., Finoguenov, A., Kodama, T., Nakata, F., & Rosati, P. 2009, *A&A*, 507, 671
- Tanaka, M., Finoguenov, A., Kodama, T., Koyama, Y., Maughan, B., & Nakata, F. 2009, *A&A*, 505, L9
- Tanaka, M., et al. 2008, *A&A*, 489, 571
- Tanaka, M., Hoshi, T., Kodama, T., & Kashikawa, N. 2007, *MNRAS*, 379, 1546
- Tanaka, M., Kodama, T., Kajisawa, M., Bower, R., Demarco, R., Finoguenov, A., Lidman, C., & Rosati, P. 2007, *MNRAS*, 377, 1206
- Tanaka, M., Kodama, T., Arimoto, N., & Tanaka, I. 2006, *MNRAS*, 365, 1392
- Tanaka, M., Kodama, T., Arimoto, N., Okamura, S., Umetsu, K., Shimasaku, K., Tanaka, I., & Yamada, T. 2005, *MNRAS*, 362, 268
- Tran, K.-V. H., Saintonge, A., Moustakas, J., Bai, L., Gonzalez, A. H., Holden, B. P., Zaritsky, D., & Kautsch, S. J. 2009, *ApJ*, 705, 809
- Tresse, L., Maddox, S., Loveday, J., & Singleton, C. 1999, *MNRAS*, 310, 262
- Verdugo, M., Ziegler, B. L., & Gerken, B. 2008, *A&A*, 486, 9
- Villar, V., Gallego, J., Pérez-González, P. G., Pascual, S., Noeske, K., Koo, D. C., Barro, G., & Zamorano, J. 2008, *ApJ*, 677, 169
- Westra, E., Geller, M. J., Kurtz, M. J., Fabricant, D. G., & Dell'Antonio, I. 2010, *ApJ*, 708, 534
- White, S. D. M., et al. 2005, *A&A*, 444, 365
- Wilman, D. J., Oemler, A., Mulchaey, J. S., McGee, S. L., Balogh, M. L., & Bower, R. G. 2009, *ApJ*, 692, 298
- Wilman, D. J., et al. 2008, *ApJ*, 680, 1009
- Wolf, C., et al. 2009, *MNRAS*, 393, 1302
- Wolf, C., Gray, M. E., & Meisenheimer, K. 2005, *A&A*, 443, 435
- Yagi, M., Kashikawa, N., Sekiguchi, M., Doi, M., Yasuda, N., Shimasaku, K., & Okamura, S. 2002, *AJ*, 123, 66
- Yoshida, M., et al. 2006, *ApJ*, 653, 988
- Zheng, X. Z., Bell, E. F., Papovich, C., Wolf, C., Meisenheimer, K., Rix, H.-W., Rieke, G. H., & Somerville, R. 2007, *ApJ*, 661, L41